Quantum Memristors with Quantum Computers

Y.-M. Guo,[1,*] F. Albarrán-Arriagada,[2,3] H. Alaeian,[4] E. Solano,[1,5,6,†] and G. Alvarado Barrios[1,‡]

[1] *International Center of Quantum Artificial Intelligence for Science and Technology (QuArtist) and Physics Department, Shanghai University, Shanghai 200444, China*

[2] *Departamento de Física, Universidad de Santiago de Chile (USACH), Avenida Víctor Jara 3493, Santiago 9170124, Chile*

[3] *Center for the Development of Nanoscience and Nanotechnology, Estación Central 9170124, Chile*

[4] *Elmore Family School of Electrical and Computer Engineering, Department of Physics and Astronomy, Purdue Quantum Science and Engineering Institute, Purdue University, West Lafayette, Indiana 47907, USA*

[5] *IKERBASQUE, Basque Foundation for Science, Plaza Euskadi 5, Bilbao 48009, Spain*

[6] *Kipu Quantum, Kurwenalstrasse 1, Munich 80804, Germany*

(Received 12 January 2022; revised 25 April 2022; accepted 20 July 2022; published 31 August 2022)

We propose the encoding of memristive quantum dynamics on a digital quantum computer. Using a set of auxiliary qubits, we simulate an effective non-Markovian environment inspired by a collisional model, reproducing memristive features between expectation values of different operators in a single qubit. We numerically test our proposal in an IBM quantum simulator with 32 qubits, obtaining a pinched hysteresis curve that characterizes our quantum memristor model. Furthermore, we extend our method to the case of two coupled quantum memristors, opening the door to the study of neuromorphic quantum computing in the current noisy devices.

DOI: 10.1103/PhysRevApplied.18.024082

I. INTRODUCTION

The study of resistive memories dates back to the 1950s, to Kubo's response theory [1]. In 1971, the concept of the "memristor" was introduced by Leon Chua [2,3] referring to a resistive memory described as a two-terminal passive circuit element relating the charge and the flux. As a consequence of this relation, the current across the device depends on the history of charges that have passed through it. Specifically, a voltage-controlled memristor has the circuit variable relations

$$I(t) = M(q)V(t),$$
$$q = \int I(t)dt. \tag{1}$$

The memductance $M(q)$ depends on the internal state given by the charge q, which depends on the history of the current flowing through the device. With this state-dependent Ohm's law, the independent variable $V(t)$ and dependent variable $I(t)$ constitute the input and output of a memristor, respectively.

The experimental study of resistive memories was initiated by Hickmott [4] in 1962 by observing hysteretic behavior in oxide insulators. In 2008, the Hewlett-Packard laboratories showed an example of a memristor [5,6] and, since then, the field of memristive devices has developed substantially [7–10]. These devices possess memory effects and a nonlinear current-voltage relationship. In this sense, they are one of the leading candidates for the implementation of neuromorphic computers [11–13] that may overcome the von Neumann bottleneck [14].

Given the promising prospects of a memristor as a fundamental element for neuromorphic classical computing, it is natural to ask whether it is possible to design a quantum version of this element and explore its properties. In recent years, several theoretical efforts have investigated this question [15–19], with the implementation of memory-based protocols for quantum advantage [20,21] and, recently, the implementation of a quantum memristive device in a photonic platform [22]. The latter work has, remarkably, proposed possible applications of quantum memristors in quantum machine-learning tasks by means of reservoir computing, where quantum memristors can outperform their classical counterparts. Nevertheless, the implementation of small quantum memristive networks has eluded experimental efforts due to the difficulty involved in coupling quantum memristive devices.

On the other hand, universal quantum computers offer the possibility of simulating complex system dynamics in a digital way [23]. Therefore, the existing technologies allow the experimental realization of small and noisy

*phys.yimingguo@gmail.com
†enr.solano@gmail.com
‡phys.gabriel@gmail.com

quantum devices as good candidates for quantum simulations of complex quantum dynamics with unitary gates. However, quantum memristive systems involve nonunitary dynamics of a non-Markovian nature. The latter can be obtained from the unitary dynamics of a larger system, tracing some degrees of freedom associated with auxiliary subsystems commonly called the environment. This means that we can obtain effective families of nonunitary and non-Markovian dynamics in quantum computers by considering a subset of quantum processor qubits [24,25].

In this paper, we simulate the dynamics of a quantum memristor on a quantum computer by digitally implementing its open-system dynamics. We test our protocol for a single two-level quantum memristor in the IBM quantum simulator *ibmq_qasm* [26] with 32 qubits. In addition, we study coupled quantum memristors with a variety of possible interactions. This work showcases how quantum computers can be used as a test bed for studying individual and coupled quantum memristors, a step toward thorough studies of memristor-based neuromorphic quantum computing.

The paper is organized as follows. In Sec. II, we present the model of a two-level quantum memristor. In Sec. III, we describe the developed protocols for the digital simulation of the single and coupled quantum memristors, in general, and demonstrate the feasibility of the algorithm by showing several examples. Section IV concludes this work and presents further possible developments.

II. TWO-LEVEL QUANTUM MEMRISTOR

For the simulation, we consider a quantum memristor model that can be implemented in a two-level system. As a starting point, it has been shown that a quantum harmonic oscillator with a tunable decay rate can represent a quantum memristor [16,18] provided that the decay rate is driven so as to satisfy memristive equations. Here, the system can be described by the master equation

$$\frac{\partial}{\partial t}\hat{\rho} = -\frac{i}{\hbar}[\hat{H},\hat{\rho}] + \Gamma(t)\left(\hat{a}\hat{\rho}\hat{a}^{\dagger} - \frac{1}{2}\hat{a}^{\dagger}\hat{a}\hat{\rho} - \frac{1}{2}\hat{\rho}\hat{a}^{\dagger}\hat{a}\right), \tag{2}$$

where $\hat{H} = \hbar\omega(\hat{a}^{\dagger}a + 1/2)$ and $\Gamma(t) > 0$.

The memristive variables can be written as

$$\begin{aligned}\langle\hat{u}\rangle &= -\frac{1}{2}\sqrt{\frac{m\hbar\omega}{2}}\left\langle i(\hat{a}^{\dagger} - \hat{a})\right\rangle,\\ \langle\hat{O}\rangle &= \sqrt{\frac{m\hbar\omega}{2}}\frac{d}{dt}\left\langle i(\hat{a}^{\dagger} - \hat{a})\right\rangle - \sqrt{\frac{m\omega}{2\hbar}}\left\langle(\hat{a}^{\dagger} + \hat{a})\right\rangle,\end{aligned} \tag{3}$$

where $\langle\hat{u}\rangle$ and $\langle\hat{O}\rangle$ are the input and output variables of the quantum memristor. Using Eq. (2), for the time derivative of the expectation value in Eq. (3), it can be shown that the output is related to the input by the expression

$$\langle\hat{O}\rangle = G(t)\langle\hat{u}\rangle, \tag{4}$$

where $G(t) = \alpha\Gamma(t)$ is the memductance and α is a constant. This equation has the same form as Eq. (1), which is a case of memristive behavior; therefore, this system corresponds to a quantum memristor. In this case, when the input $\langle\hat{u}\rangle$ has a sinusoidal time dependence, the output $\langle\hat{O}\rangle$ as a function of the input $\langle\hat{u}\rangle$ traverses a pinched hysteresis loop that characterizes this quantum memristor. Note that we are not considering an external energy source; thus the system loses its energy continuously and the number of excitations in the oscillator, $\langle\hat{a}^{\dagger}\hat{a}\rangle$, decays in time.

If we consider only one excitation in the initial state, at zero temperature, the dynamics can be approximated with a two-level system, where the Hamiltonian reads

$$\hat{H}_2 = \hbar\omega\left(\hat{\sigma}_{+}\sigma_{-} + \frac{1}{2}\right) = \frac{1}{2}\hbar\omega\left(\hat{\sigma}_z + 2\right) \tag{5}$$

and the master equation becomes

$$\frac{\partial}{\partial t}\hat{\rho}_2 = -\frac{i}{\hbar}[\hat{H}_2,\hat{\rho}_2] + \Gamma(t)\left(\hat{\sigma}_{-}\hat{\rho}_2\hat{\sigma}_{+} - \frac{1}{2}\{\hat{\sigma}_{+}\hat{\sigma}_{-},\hat{\rho}_2\}\right), \tag{6}$$

where $\hat{\sigma}_{+}$, $\hat{\sigma}_{-}$, and σ_z are the Pauli raising, lowering, and Z operators, respectively.

Now, we can implement the memristive dynamics by controlling $\Gamma(t)$ and, in order to be able to compare our results with that of previous literature, we consider a time-dependent decay rate as given by Ref. [18]. This corresponds to a conductance-asymmetric superconducting quantum interference device (SQUID) quantum memristor, where the decay rate, $\Gamma(t)$, is associated with quasiparticle decay, which reads

$$\Gamma(t) = \gamma_0(1 - \sin[\cos(\omega t)]), \tag{7}$$

where γ_0 is a constant associated with the decay strength. In Ref. [18], the input and output variables correspond to voltage $\langle\hat{V}\rangle$ and current $\langle\hat{I}\rangle$, respectively; we use the same notation to facilitate the comparison in later sections. Thus, following Eq. (3), the memristive variables can be written as

$$\begin{aligned}\langle\hat{V}_2\rangle &= -\frac{1}{2}\sqrt{\frac{m\hbar\omega}{2}}\langle\hat{\sigma}_y\rangle,\\ \langle\hat{I}_2\rangle &= \sqrt{\frac{m\hbar\omega}{2}}\frac{d}{dt}\langle\hat{\sigma}_y\rangle - \sqrt{\frac{m\omega}{2\hbar}}\langle\hat{\sigma}_x\rangle.\end{aligned} \tag{8}$$

Now, the memristive equation reads

$$\langle\hat{I}_2\rangle = \Gamma(t)\langle\hat{V}_2\rangle. \tag{9}$$

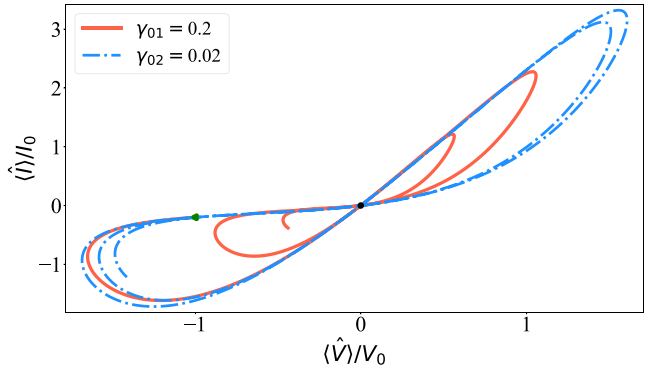

FIG. 1. The I-V characteristics of the two-level quantum memristors for two cases. For both quantum memristors, $m = 1$, $\hbar = 1$, and $\omega = 1$, with the same initial state $|\psi_0\rangle = \cos(\pi/8)|e\rangle + \sin(\pi/8)e^{(i\pi/5)}|g\rangle$ and different decay rates $\gamma(t)$, as shown in Eq. (7), $\gamma_{01} = 0.2$ (solid red line) and $\gamma_{02} = 0.02$ (dashed-dotted blue line). The expectation values are normalized to the initial values shown by the green dot, i.e., $V_0 = |\langle\hat{V}\rangle|_{t=0}$ and $I_0 = |\langle\hat{I}\rangle|_{t=0}$. In both cases, the I-V curves show a pinched hysteresis loop, denoted by the black dot in the figure.

As an example, we numerically solve Eq. (6) for different values of γ_0. In Fig. 1, we plot the corresponding current-voltage (I-V) curves, showing the characteristic pinched hysteresis loop. In the figure, the red curve shrinks faster than the blue curve due to its larger decay rate. In both cases, the system is initialized in a pure state as $|\psi_0\rangle = \cos(\pi/8)|e\rangle + \sin(\pi/8)e^{i\pi/5}|g\rangle$.

In Sec. III, we show how the two-level quantum memristive dynamics can be simulated on a digital quantum computer using one qubit as the memristive system (the system qubit) and a set of auxiliary qubits as a non-Markovian reservoir.

III. QUANTUM CIRCUITS FOR MEMRISTIVE DYNAMICS

A. Single memristive dynamics

We describe how to map the memristive dynamics of Eq. (6) on a quantum circuit, where each digital step corresponds to a set of operations evolving the system qubit state from time t_i to time t_{i+1}. The whole time evolution, therefore, can be simulated by the repeated application of these digital steps. This method can also be extended to incorporate interactions between memristors, as we show later.

We start by writing the master equation of Eq. (6) in the interaction picture

$$\partial_t\hat{\rho}_I = \gamma(t)\left(\hat{\sigma}_-\hat{\rho}_I\hat{\sigma}_+ - \frac{1}{2}\{\hat{\sigma}_+\hat{\sigma}_-,\hat{\rho}_I\}\right), \tag{10}$$

where $\hat{\rho}_I(t) = e^{it/\hbar\hat{H}}\hat{\rho}_2(t)e^{-it/\hbar\hat{H}}$ and $\hat{H} \equiv \hat{H}_2$. At zero temperature, this system has an exact solution (see Ref. [24]) as

$$\hat{\rho}_I(t) = \begin{pmatrix} |c_1(t)|^2 & c_0^* c_1(t) \\ c_0 c_1(t)^* & 1 - |c_1(t)|^2 \end{pmatrix}, \tag{11}$$

where

$$\gamma(t) = -2\mathrm{Re}\left\{\frac{\dot{c}_1(t)}{c_1(t)}\right\}, \tag{12}$$

and c_0 is determined by the initial state. Without loss of generality, we assume $c_1(t)$ to be a real number, obtaining the density matrix

$$\hat{\rho}_I(t) = \begin{pmatrix} c_1(t)^2 & c_0^* c_1(t) \\ c_0 c_1(t) & 1 - c_1(t)^2 \end{pmatrix}. \tag{13}$$

Finally, Eq. (12) can be used to solve for $c_1(t)$ as

$$c_1(t) = c_1(0)e^{\kappa(t)},$$
$$\kappa(t) = \frac{-\int_0^t \gamma(t')dt'}{2}. \tag{14}$$

If the initial state is a pure state of the form $|\psi_0\rangle = \cos(a)|e\rangle + \sin(a)e^{ib}|g\rangle$, the density matrix at time t has the form

$$\hat{\rho}_I(t) = \begin{pmatrix} (\cos a e^{\kappa(t)})^2 & \cos a \sin a e^{ib} e^{\kappa(t)} \\ \cos a \sin a e^{-ib} e^{\kappa(t)} & 1 - (\cos a e^{\kappa(t)})^2 \end{pmatrix}, \tag{15}$$

where $a \in [0, \pi/2]$ and $b \in [0, 2\pi]$.

We can also write the dynamical map defined by the master equation in Eq. (10), corresponding to an amplitude-damping mechanism, using its Krauss operators [27] as

$$\hat{\rho}_I(t) = \varepsilon_{t,0}[\hat{\rho}_I(0)] = \hat{E}_0^{(0,t)}\hat{\rho}_I(0)(\hat{E}_0^{(0,t)})^\dagger + \hat{E}_1^{(0,t)}\hat{\rho}_I(0)(\hat{E}_1^{(0,t)})^\dagger,$$
$$\hat{E}_0^{(0,t)} = \begin{pmatrix} e^{\kappa(t)} & 0 \\ 0 & 1 \end{pmatrix}, \hat{E}_1^{(0,t)} = \begin{pmatrix} 0 & 0 \\ \sqrt{1 - e^{2\kappa(t)}} & 0 \end{pmatrix}. \tag{16}$$

Since the map of Eq. (16) gives us the density matrix in the interaction picture, we must transform it back to the Schrödinger picture using $\hat{\rho}_2(t) = e^{-it/\hbar\hat{H}}\hat{\rho}_I(t)e^{it/\hbar\hat{H}}$, to calculate the expectation values of the two-level quantum memristor.

To mimic the action of the operators $\hat{E}_0$ and $\hat{E}_1$, we consider the gate circuit shown in Fig. 2. The different blocks in the figure represent the different operations on the qubits. Each line represents a qubit register and the dashed line indicates a classical bit register, which can store measurement results. Our gate-circuit algorithm is realized with the

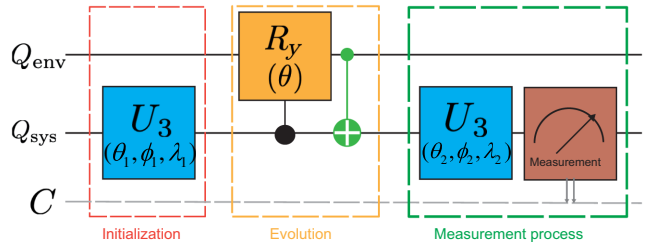

FIG. 2. The proposed circuit for a single-time-step quantum memristor simulation with three basic steps of initialization, evolution, and the measurement process. The circuit consists of single-qubit gates, i.e., unitary gate (U3, in blue) and two-qubit gates, i.e., a control-rotation-Y ($\mathrm{CR_y}$) gate (in yellow) and a controlled-NOT (CNOT) gate (in green). The last step is a measurement process.

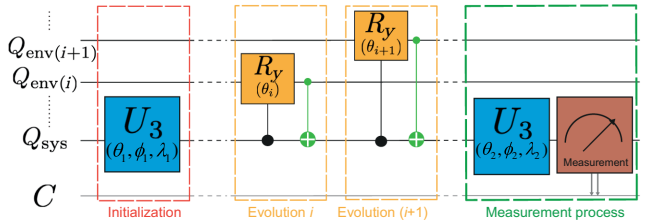

FIG. 3. The proposed circuit for the digitized dynamics simulation. As an extension of the circuit shown in Fig. 2, the evolution step is repeated n times before the measurement process.

IBM QISKIT package [28], a PYTHON-based programming language for the IBM Q Experience [26].

This gate-based circuit is split into three basic steps. First, there is the initialization, where we prepare the qubit $Q_{\rm sys}$ in its initial state, $|\psi_0\rangle$, and the auxiliary qubits ($Q_{\rm env}$) are initialized in the state $|0\rangle$. Second, there is the evolution step, where we entangle the system and environment qubits, using a controlled rotation around the y axis, with and angle $\theta = \arccos(e^{\kappa(t)})$. Here, we use as target the auxiliary qubit $Q_{\rm env}$ and then a controlled-NOT (CNOT) gate using as target the system qubit $Q_{\rm sys}$. At this point, the state of $Q_{\rm sys}$ corresponds to $\rho_I(t)$ in Eq. (16), which corresponds to the state at t. Third, there is the measurement step, where we measure $\hat{\sigma}_x$ or $\hat{\sigma}_y$, related to the expectation values of the memristor current and voltage as in Eq. (8).

Similarly, if we change the rotation angle θ in the evolution step, we can obtain the effective transformation from t_i to t_{i+1}. To do this, we consider

$$\kappa(t_{i+1},0) = \frac{-\int_0^{t_{i+1}}\gamma(t')dt'}{2}, \quad \kappa(t_i,0) = \frac{-\int_0^{t_i}\gamma(t')dt'}{2}. \tag{17}$$

Then, we can calculate $\hat{\rho}_I(t_{i+1})$ and $\hat{\rho}_I(t_i)$ with Eq. (16). Using the density matrices at times t_i and t_{i+1}, we can find the dynamical map from t_i to t_{i+1} as

$$\begin{aligned}\hat{\rho}_I(t_{i+1}) &= \varepsilon_{t_{i+1},t_i}[\hat{\rho}_I(t_i)] \\ &= \hat{E}_0^{(t_i,t_{i+1})}\hat{\rho}_I(0)(\hat{E}_0^{(t_i,t_{i+1})})^\dagger \\ &\quad + \hat{E}_1^{(t_i,t_{i+1})}\hat{\rho}_I(0)(\hat{E}_1^{(t_i,t_{i+1})})^\dagger,\end{aligned} \tag{18}$$

where $\kappa(t_{i+1},t_i) = -\int_{t_i}^{t_{i+1}}\gamma(t')dt'/2$, with $E_{0(1)}$ defined in Eq. (16). Therefore, in our digital simulation, $\varepsilon_{t_{i+1},t_i}$ is the superoperator for the memristive dynamics from t_i to t_{i+1}. The quantum circuit corresponding to this method is shown in Fig. 3, which is an extension of the circuit of Fig. 2. We require one ancillary qubit for each time step $\varepsilon_{t_{i+1},t_i}$ of the memristive qubit $Q_{\rm sys}$. We can see that the rotation angle $\theta = \arccos[e^{\kappa(t_i,t_{i+1})}]$ only depends on the decay rate $\gamma(t)$ and the time steps. By measuring the expectation value of $\hat{\sigma}_x$ and $\hat{\sigma}_y$ after each step, we can obtain the evolution of the memristive variables in Eq. (8).

In Fig. 4, we show that the digital quantum simulation of a single quantum memristor compares well with the direct numerical solution of the master equation of Eq. (6). As can be seen, both the time evolution in Fig. 4(a) as well as the memristor I-V characteristics in Fig. 4(b) are well captured by our simulation protocol. Since the quantum memristor current calculation requires a time derivation, Eq. (3), the simulation precision depends on the time resolution. In our calculations, we choose 30 points per period of oscillation. We note that the source of noise in the simulator is given by the statistical error due to the finite number of shots (measurements) to estimate the expectation value and the time derivatives. We use 50 000 shots, obtaining a more realistic curve.

B. Interaction between two memristors

So far, we have investigated a single quantum memristor dynamics simulation suitable for a digital quantum computer with a few qubits. However, the implementation of a neuromorphic quantum computer requires the coupling of many such memristive quantum devices. This is a largely unexplored area and only a few efforts have been made to understand the quantum correlations and quantumness in a network of coupled quantum memristors [29]. The digital quantum simulation of memristive quantum dynamics, as proposed here, allows one to explore many different types of coupling in a quantum computer. Below, we study several possible couplings between the quantum memristors, utilizing the versatility provided by our proposed quantum simulations.

By increasing the qubit lines in the circuit of Fig. 3, we can simulate the dynamics of several quantum memristors and add interactions in each digital time step. This is shown in the circuit of Fig. 5, where the interaction operation $\hat{A}$ is applied at the end of each time step t_i. By denoting the general expression of the two-qubit interaction as $\hat{A}$, we

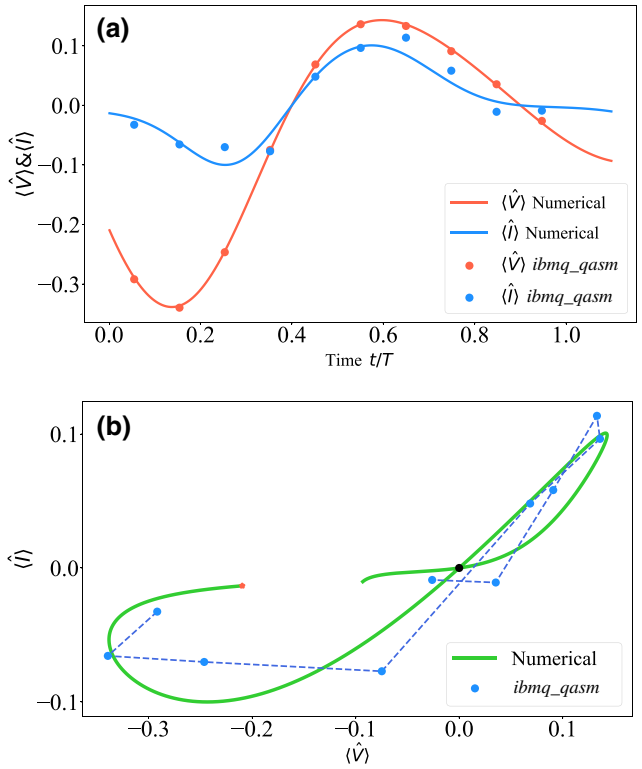

FIG. 4. (a) The expectation values of the normalized current and voltage obtained from the digital (points) and numerical (lines) methods. The parameters are $m = 1$, $\hbar = 1$, $\omega = 1$, and $\gamma_0 = 0.4$ and the initial state is $|\psi_0\rangle = \cos(\pi/4)|e\rangle + \sin(\pi/4)e^{(i\pi/5)}|g\rangle$. (b) The I-V characteristics determined from the numerical (green line) and digital (blue points) methods. The red point denotes the starting point and the black point shows zero, the hallmark of a pinched hysteresis loop of the memristor.

can write the evolution from time step t_i to t_{i+1} as

$$\hat{\rho}_I'(t_{i+1}) = \hat{A}^\dagger \hat{\rho}_I(t_{i+1})\hat{A},$$
$$\hat{\rho}_I(t_{i+1}) = \varepsilon_{1;t_i,t_{i-1}} \otimes \varepsilon_{2;t_i,t_{i-1}} \left(\hat{\rho}_I'(t_i)\right), \tag{19}$$

where the subscript index in the dynamical map means that it acts only on subsystem 1 (2) while the interaction gate $\hat{A}$ acts over both qubits, i.e., $Q_{\rm sys1}$ and $Q_{\rm sys2}$.

Since the coupling of quantum memristors affects their individual hysteresis curves in nontrivial ways, we can characterize this effect by the form factor, F, defined as

$$F = 4\pi \frac{S}{P^2}, \tag{20}$$

which measures the form of a closed loop, where S is the area enclosed by one loop in the hysteresis curve and P is its corresponding perimeter. We choose the form factor, as it has been shown that the area enclosed by the hysteresis curve is directly related to the memristor memory effects [30–32].

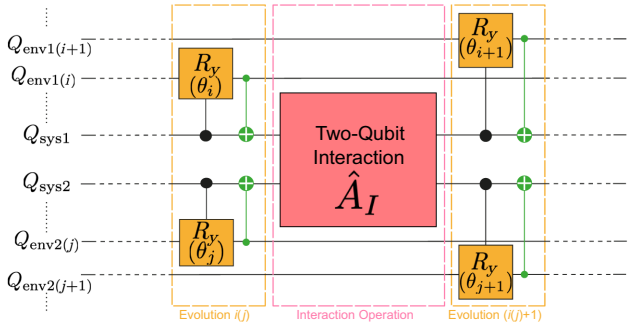

FIG. 5. The coupling operation in the circuit. Each of the qubits, $Q_{\rm sys1}$ and $Q_{\rm sys2}$, undergoes individual time evolution followed by their interaction, denoted by $\hat{A}$.

In what follows, we study two types of interaction; first, a native interaction given by the circuit implementation of the interaction Hamiltonian natural to this class of quantum memristor [29]; and, second, a non-native interaction given by other combinations of gates that do not represent the interactions that can be achieved in the architecture of superconducting quantum memristors. Here, we discuss the cases that can preserve the memristive dynamics of each memristor, while several other cases are shown in the Appendix.

1. Native interaction

For this first class, we consider the gate decomposition of the unitary operation, given by

$$\hat{U} = e^{-i\delta\hat{\sigma}_i\otimes\hat{\sigma}_i}, \quad (i = x, y, z), \tag{21}$$

which acts on the composite system, where δ is related to the coupling strength and the interaction time. In our digital-circuit implementation, this unitary operation can be realized by adding a two-qubit gate between the two quantum memristive lines as shown in Fig. 6.

As an example, we consider the case of the $\hat{\sigma}_y \otimes \hat{\sigma}_y$ interaction, which corresponds to the coupling between the internal variable in a asymmetric SQUID quantum memristor. In Fig. 7, we show the I-V hysteresis plot for each subsystem, with identical initial states. For clarity, we plot the first seven oscillations of the input, $\langle\hat{V}\rangle$, with period T

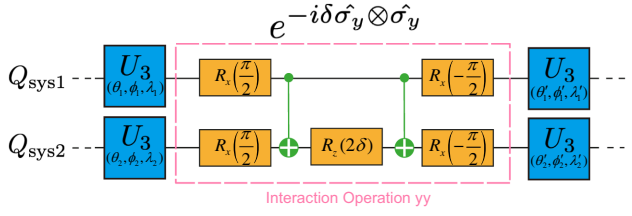

FIG. 6. The implementation of a native interaction between two coupled quantum memristors in a digital quantum circuit.

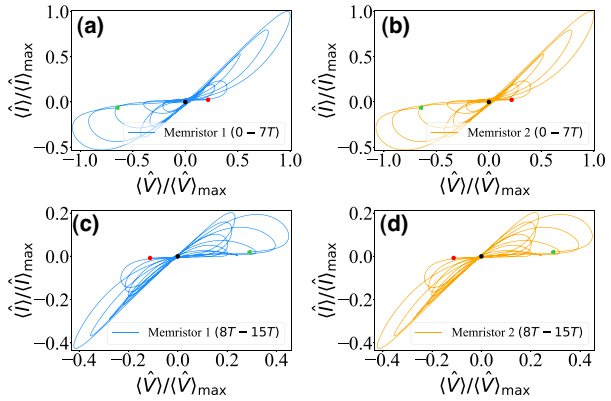

FIG. 7. The I-V curves for two coupled quantum memristors with a $\hat{\sigma}_y \otimes \hat{\sigma}_y$ interaction. In each figure, the curve starts from the green point and ends at the red point. The black circle denotes the zero point at which the hysteresis curves pinch. The expectation values of $\hat{I}$ and $\hat{V}$ are normalized by the maximum values. For both subsystems, we select $|\psi_0\rangle = 1/\sqrt{2}(|e\rangle + |g\rangle)$ as the initial state and they both have the same decay rate, $\gamma_0 = 0.02$. With the same parameters and symmetric interaction, both subsystems have the same dynamics and behavior of the expectation value.

for memristors 1 and 2 in Figs. 7(a) and 7(b), respectively. In the same way, we plot from oscillation 8 to oscillation 15 in Figs. 7(c) and 7(d). We can see that the interaction changes the memristive behavior when compared to the uncoupled case but that each subsystem still shows a pinched hysteresis curve; thus, they preserve their original memristive properties. Note that we observe a pinched hysteresis curve that is displaced from the origin; the displacement can be associated with capacitive effects that lead to similar behavior in classical devices [33]. The link to capacitive effects lies in the fact that the $\sigma_y \otimes \sigma_y$ interaction can be regarded as a capacitive coupling between the memristors in superconducting circuits.

In addition, we calculate the concurrence of the composite system and the form factor, shown in Fig. 8. We can observe entanglement sudden death (ESD) and entanglement sudden birth (ESB) during the time evolution and the behavior is inversely proportional to the form factor, which recovers the results obtained in Ref. [29].

2. Non-native interaction

Next, we analyze the non-native interaction between the two quantum memristors, which we consider as controlled two-qubit logical gates. The study of these cases is relevant since it can help us to understand the mechanisms of manipulating the memristivity.

We consider interaction operators of the form

$$\hat{C}_{Ri} = |e\rangle\langle e| \otimes \hat{R}_i(\delta) + |g\rangle\langle g| \otimes 1, \quad (i = x, y, z), \quad (22)$$

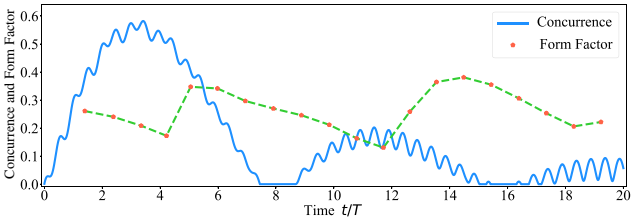

FIG. 8. The concurrence and the form factor of the composite quantum memristive system shown in Fig. 7 as a function of time. During the 20 hysteretic loops, we obtain two significant peaks, one from $t = 0$ to $t = 7T$ and the other from $t = 8T$ to $t = 15T$.

where $\hat{R}_i(\delta)$ denotes rotation gates around a different axis corresponding to three different rotation directions in the Bloch sphere for a single qubit. For the case of controlled operations, one of the quantum memristors is chosen as control and the other as target system. The effect of the interaction between the two quantum memristors strongly depends on the state of the control quantum memristor.

As an example, we consider the controlled-Y (CY) gate as the interaction between the two subsystems. Figure 9 shows the corresponding I-V curve for each quantum memristor for 20 oscillations. Figure 9(a) shows the I-V curve for the quantum memristor corresponding to the control qubit and Fig. 9(b) shows the I-V curve for the target qubit. With the implementation of such an asymmetric interaction, the resulting hysteresis curve is very different for each subsystem even when both have the same initial state. Here, the control memristive system has a bias in its loop for every period and, therefore, it shows a memristive behavior that is not present in its components. In contrast, subsystem 2 retains the memristive behavior. This can be understood as the target memristor perceiving the interaction with the control memristor as an additional collision with an environment, which distorts the hysteresis curve from its uncoupled form but is still perceived as the same mechanism for memristive behavior. In this case, the concurrence quickly decays to zero.

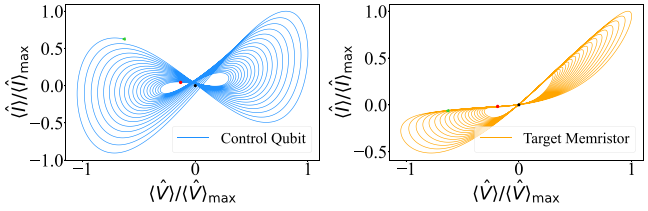

FIG. 9. The I-V curves for both subsystems with 20 oscillation periods. With the asymmetric interaction CR_y, the two subsystems are changing differently. Both qubits start from the initial state $|\psi_0\rangle = 1/\sqrt{2}(|e\rangle + |g\rangle)$ and they have the same decay rate, $\gamma_0 = 0.02$. The dynamics of both start from the green triangle, while the black circle is the zero point.

From an experimental point of view, memristive devices have been implemented in quantum platforms such as quantum dots [34] and photonic architectures [22]. In the first case, two quantum dots (a memristive one and an auxiliary one) are connected capacitively and, using a tunnel barrier to electronic reservoirs, in such a system the current through the memristive quantum dot depends on the occupancy state of the auxiliary quantum dot, which provides a memristive feedback relation. In the second case, a photonic quantum state is split using a beam splitter and then the transmittance of the beam splitter is changed according to the outcome of the measurement in one of the output branches, inducing a memristive relation in the other output branch. Also, another interesting system with memory effects comes from the so-called "membosonsampling" proposal [20]. In this experiment, one input mode in a photonic chip has information from past instances of the output probabilities, providing a new task for quantum advantage. On the other hand, other memristive systems have been proposed theoretically, from superconducting circuits [15,18], where the memristive relation appears naturally from a conductance-asymmetric SQUID, movement equations for which are simulated in this work in a quantum computer, to polariton-based systems [35], where the memristive relation comes from the interaction with an auxiliary system. Finally, proposals also exist for the composition of quantum memristors to use quantum correlation properties based on the conductance-asymmetric SQUID memristor [29].

Finally, we briefly discuss the possible applications of quantum memristors. It has been theoretically proposed [22] that quantum memristors in parallel can compose the reservoir in reservoir computing for quantum machine-learning tasks. In order to be effective, this technique requires high dimensionality, nonlinearity, and memory in the reservoir. Remarkably, it has been shown that quantum memristors outperform classical memristors for tasks such as image classification. This highlights the importance of quantum effects in memristors for the design of future neuromorphic computing applications. Note also that memristors need not only be considered as possible candidates for artificial neurons, which are the main use of their classical counterparts.

IV. CONCLUSIONS

We design a quantum algorithm to simulate memristive quantum dynamics on a digital quantum computer. Our protocol employs a set of auxiliary qubits to simulate an effective environment that generates memristive quantum features in the expectation value of different operators in a single qubit. The memristive quantum dynamics have been obtained using each auxiliary qubit to evolve the system by one time step. We simulate our protocol using an IBM quantum simulator with 32 qubits and observe the hysteresis curve that characterizes the memristive quantum behavior of our model. The statistical noise given by the total number of measurement shots, used to estimate the different expectation values, is the fundamental error in this class of quantum simulations.

Furthermore, we consider interactions between the quantum memristors that can be achieved within the superconducting circuit architectures and also interactions outside of this range. To analyze the effect of the interaction, we calculate the entanglement between the quantum memristors and the form factor for their corresponding hysteresis curves. We find that in the case of the $\sigma_y \otimes \sigma_y$ interaction (native interaction), the memristivity is almost preserved, with a hysteresis curve that is slightly displaced from the origin. In the case of a CY interaction (non-native interaction) between quantum memristors, the memristivity is perfectly preserved for the target quantum memristor and lost for the control quantum memristor. Other cases corresponding to different interactions result in complete loss of the memristive dynamics. In general, memristive quantum dynamics are fragile to interactions. The cases that preserve the memristivity of each component can be of interest for future applications. Among them, we highlight the upcoming development of neuromorphic quantum computing for the design of quantum neural networks based on quantum memristors. In this context, neuromorphic quantum simulations provide a tool to explore coupled quantum memristive dynamics, not restricted to native interactions, in order to gain insight into the underlying mechanisms of quantum memristors.

ACKNOWLEDGMENTS

We acknowledge the financial support from Science and Technology Commission of Shanghai Municipality (STCSM) projects 2019SHZDZX01-ZX04 and 20DZ2290900, Agencia Nacional de Investigación y Desarrollo (ANID) Subvención a la Instalación en la Academia SA77210018, ANID Proyecto Basal AFB 180001, and the Purdue University Startup fund.

APPENDIX: COUPLED QUANTUM MEMRISTORS—OTHER CASES

We show further cases for the interaction of quantum memristors. We classify them as the native interaction and the non-native interaction.

1. Native interaction

We consider the $\sigma_x \otimes \sigma_x$ and $\sigma_z \otimes \sigma_z$ interaction. Figures 10(a) and 10(b) show the I-V curves for the $\sigma_x \otimes \sigma_x$ interaction for each quantum memristor and Figures 10(c) and 10(d) show the I-V curves for the $\sigma_z \otimes \sigma_z$ interaction. Note

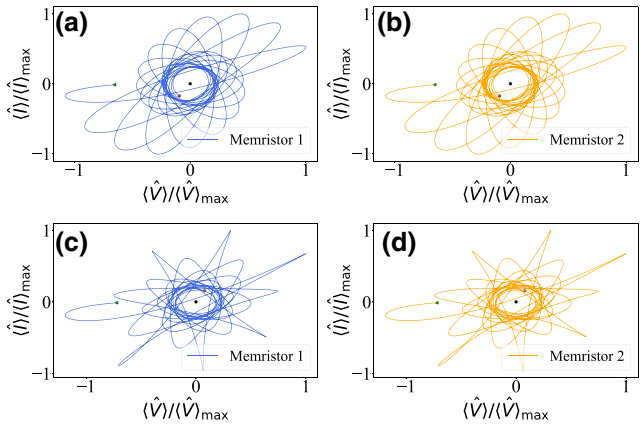

FIG. 10. The I-V curve of the (a),(b) $\hat{\sigma}_x \otimes \hat{\sigma}_x$ and (c),(d) $\hat{\sigma}_z \otimes \hat{\sigma}_z$ interactions. We consider 20 oscillations of $\langle \hat{V} \rangle$ for both cases. We select $|\psi_0\rangle = 1/\sqrt{2}(|e\rangle + |g\rangle)$ as the initial state and they both have the same decay rate, $\gamma_0 = 0.02$.

that in these cases the interaction completely destroys the memristive dynamics.

2. Non-native interaction

We consider the controlled-X (CX), controlled-Z (CZ), and partial-SWAP interactions. The corresponding I-V curve for each quantum memristor is shown in Fig. 11.

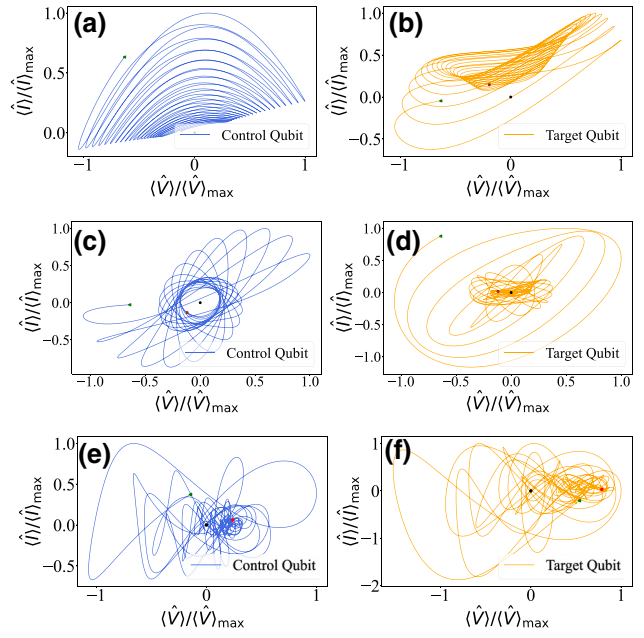

FIG. 11. The I-V curves of the (a),(b) Controlled-Rotation-X, (c),(d) Controlled-Rotation-Z, and (e),(f) partial-SWAP interactions. We considered 20 oscillations of $\langle \hat{V} \rangle$ for both cases. We select $|\psi_0\rangle = 1/\sqrt{2}(|e\rangle + |g\rangle)$ as the initial state, where both have the same decay rate, $\gamma_0 = 0.02$.

Again, in these cases the interaction completely destroys the memristive dynamics.

[1] R. Kubo, Statistical-mechanical theory of irreversible processes. I. General theory and simple applications to magnetic and conduction problems, J. Phys. Soc. Jpn. **12**, 570 (1957).

[2] L. Chua, Memristor—The missing circuit element, IEEE Trans. Circuit Theory **18**, 507 (1971).

[3] L. O. Chua and S. M. Kang, Memristive devices and systems, Proc. IEEE **64**, 209 (1976).

[4] T. W. Hickmott, Low-frequency negative resistance in thin anodic oxide films, J. Appl. Phys. **33**, 2669 (1962).

[5] R. Waser and M. Aono, Nanoionics-based resistive switching memories, Nat. Mater. **6**, 833 (2007).

[6] D. B. Strukov, G. S. Snider, D. R. Stewart, and R. S. Williams, The missing memristor found, Nature **453**, 80 (2008).

[7] A. Thomas, Memristor-based neural networks, J. Phys. D: Appl. Phys. **46**, 093001 (2013).

[8] R. Marani, G. Gelao, and A. G. Perri, A review on memristor applications (2015), ArXiv:1506.06899.

[9] I. Vourkas and G. C. Sirakoulis, Emerging memristor-based logic circuit design approaches: A review, IEEE Circuits Syst. Mag. **16**, 15 (2016).

[10] Y. Li, Z. Wang, R. Midya, Q. Xia, and J. J. Yang, Review of memristor devices in neuromorphic computing: Materials sciences and device challenges, J. Phys. D: Appl. Phys. **51**, 503002 (2018).

[11] Z. Wang, S. Joshi, S. E. Savel'ev, H. Jiang, R. Midya, P. Lin, M. Hu, N. Ge, J. P. Strachan, and Z. Li, *et al.*, Memristors with diffusive dynamics as synaptic emulators for neuromorphic computing, Nat. Mater. **16**, 101 (2017).

[12] P. Lin, C. Li, Z. Wang, Y. Li, H. Jiang, W. Song, M. Rao, Y. Zhuo, N. K. Upadhyay, and M. Barnell, *et al.*, Three-dimensional memristor circuits as complex neural networks, Nat. Electron. **3**, 225 (2020).

[13] P. Yao, H. Wu, B. Gao, J. Tang, Q. Zhang, W. Zhang, J. J. Yang, and H. Qian, Fully hardware-implemented memristor convolutional neural network, Nature **577**, 641 (2020).

[14] N. K. Upadhyay, H. Jiang, Z. Wang, S. Asapu, Q. Xia, and J. J. Yang, Emerging memory devices for neuromorphic computing, Adv. Mater. Technol. **4**, 1800589 (2019).

[15] S. Peotta and M. Di Ventra, Superconducting Memristors, Phys. Rev. Appl. **2**, 034011 (2014).

[16] P. Pfeiffer, I. L. Egusquiza, M. Di Ventra, M. Sanz, and E. Solano, Quantum memristors, Sci. Rep. **6**, 29507 (2016).

[17] M. Sanz, L. Lamata, and E. Solano, Invited article: Quantum memristors in quantum photonics, APL Photon. **3**, 080801 (2018).

[18] J. Salmilehto, F. Deppe, M. Di Ventra, M. Sanz, and E. Solano, Quantum memristors with superconducting circuits, Sci. Rep. **7**, 42044 (2017).

[19] T. Gonzalez-Raya, J. M. Lukens, L. C. Céleri, and M. Sanz, Quantum memristors in frequency-entangled optical fields, Materials **13**, 864 (2020).

[20] J. Gao, X.-W. Wang, W.-H. Zhou, Z.-Q. Jiao, R.-J. Ren, Y.-X. Fu, L.-F. Qiao, X.-Y. Xu, C.-N. Zhang, and X.-L. Pang,

et al., Quantum advantage with timestamp membosonsampling, Chip **1**, 100007 (2020).

[21] W.-H. Zhou, J. Gao, Z.-Q. Jiao, X.-W. Wang, R.-J. Ren, X.-L. Pang, L.-F. Qiao, C.-N. Zhang, T.-H. Yang, and X.-M. Jin, *et al.*, Timestamp boson sampling (2020), ArXiv:2009.03327.

[22] M. Spagnolo, J. Morris, S. Piacentini, M. Antesberger, F. Massa, A. Crespi, F. Ceccarelli, R. Osellame, and P. Walther, Experimental photonic quantum memristor, Nat. Photon. **16**, 318 (2022).

[23] I. M. Georgescu, S. Ashhab, and F. Nori, Quantum simulation, Rev. Mod. Phys. **86**, 153 (2014).

[24] G. García-Pérez, M. A. C. Rossi, and S. Maniscalco, IBM Q Experience as a versatile experimental testbed for simulating open quantum systems, npj Quantum Inf. **6**, 1 (2020).

[25] K. Head-Marsden, S. Krastanov, D. A. Mazziotti, and P. Narang, Capturing non-Markovian dynamics on near-term quantum computers, Phys. Rev. Res. **3**, 013182 (2021).

[26] Official web page *IBM Quantum*.

[27] M. Nielsen and I. Chuang, *Quantum Computation and Quantum Information* (Cambridge University Press, Cambridge, 2010).

[28] G. Aleksandrowicz, T. Alexander, P. Barkoutsos, L. Bello, Y. Ben-Haim, D. Bucher, F. J. Cabrera-Hernández, J. Carballo-Franquis, A. Chen, and C.-F. Chen, *et al.*, Online documentation, QISKIT: An Open-source Framework for Quantum Computing (2019).

[29] S. Kumar, F. A. Cárdenas-López, N. N. Hegade, X. Chen, F. Albarrán-Arriagada, E. Solano, and G. Alvarado Barrios, Entangled quantum memristors, Phys. Rev. A **104**, 062605 (2021).

[30] A. G. Radwan, M. A. Zidan, and K. N. Salama, *On the mathematical modeling of memristors. Int. Conf. Microelectron.*, 284 (2010).

[31] Z. Biolek, D. Biolek, and V. Biolkova, Computation of the area of memristor pinched hysteresis loop, IEEE Trans. Circuits Syst. II: Express Briefs **59**, 607 (2012).

[32] D. Biolek, Z. Biolek, and V. Biolková, Interpreting area of pinched memristor hysteresis loop, Electron. Lett. **50**, 74 (2014).

[33] B. Sun, Y. Chen, M. Xiao, G. Zhou, S. Ranjan, W. Hou, X. Zhu, Y. Zhao, S. A. T. Redfern, and Y. N. Zhou, A unified capacitive-coupled memristive model for the non-pinched current-voltage hysteresis loop, Nano Lett. **9**, 19 (2019).

[34] Y. Li, W. Holloway, S. C. Benjamin, G. A. D. Briggs, J. Baugh, and J. A. Mol, Double quantum dot memristor, Phys. Rev. B **96**, 075446 (2017).

[35] A. Norambuena, F. Torres, M. Di Ventra, and R. Coto, Polariton-Based Quantum Memristors, Phys. Rev. Appl. **17**, 024056 (2022).